

The mode-coupling crossover of glasses is a localization transition

Daniele Coslovich,¹ Andrea Ninarello,^{1,2} and Ludovic Berthier¹

¹Laboratoire Charles Coulomb (L2C), Université de Montpellier, CNRS, Montpellier, France

²CNR-ISC, Uos Sapienza, Piazzale A. Moro 2, 00185 Roma, Italy

(Dated: November 18, 2022)

We study the equilibrium statistical properties of the potential energy landscape of several glass models in a temperature regime so far inaccessible to computer simulations. We show that unstable modes of the stationary points undergo a localization transition in real space at the mode-coupling crossover temperature determined from the dynamics. The concentration of localized unstable modes found at low temperature is a non-universal, finite dimensional feature not captured by mean-field glass theory. Our findings reconcile previous conflicting numerical results and put strong constraints on theoretical descriptions of glass formation.

The formation of a glass from the supercooled melt results from a giant increase of the structural relaxation time when the temperature drops below the melting point [1, 2]. Whether the slowing down of molecular motion is driven by a single or several physical mechanisms, active over distinct temperature regimes, is still unclear. Available theories are all but unanimous [3, 4], while experiments and simulations, despite recent technical and numerical advances [5], struggle to disentangle theoretical predictions on the sole basis of relaxation data. The existence of a temperature crossover separating two physical regimes of dynamic relaxation is supported by a number of empirical observations and models, but is subject to lively debates [4]. This crossover is described as an avoided dynamic singularity by mode-coupling [6] and mean-field [7] theories of glasses.

In the early 2000's, a series of studies [8–13] suggested that this smooth dynamic crossover originates from an underlying sharp geometric transition characterizing the potential energy surface (PES). Physically, the transition is between a high-temperature regime where the dynamics takes place near unstable saddle modes and a low-temperature one where dynamics is activated between energy minima. In mean-field glass models, a geometric transition is analytically found: below a critical energy level, the closest stationary point to a typical configuration on the PES is not a saddle anymore but a local minimum [14, 15]. The existence of a sharp geometric transition was reported for several liquids with soft interactions, with universal characteristics [9–12, 16]. However, these results have been criticized at the methodological [17, 18] and conceptual levels [19], and subsequent studies did not find a transition [20–23], but the transition temperature could not be easily crossed. From these conflicting results it is difficult to draw firm conclusions on the nature of the mode-coupling crossover in actual three-dimensional liquids.

Here, we resolve these contradictions and clarify the nature of the change of the PES associated to the mode-coupling crossover in finite dimensions. Our work builds on two key enabling factors, respectively algorithmic and conceptual. The first key feature of our work is the use of an efficient swap Monte Carlo algorithm [24, 25], which en-

ables us to probe the landscape properties on both sides of the mode-coupling crossover temperature [26, 27]. Second, we recognize that the geometric transition, as obtained in mean-field models, can only concern the subset of unstable directions on the PES that correspond to *delocalized* displacements, which involve a finite fraction of particles. Previous studies of the statistics of stationary points have considered instead all unstable modes, irrespective of their spatial characteristics. Our analysis demonstrates that a sharp geometric transition occurs only for delocalized modes and that the mode-coupling temperature crossover therefore coincides with a localization transition of the unstable directions of the PES. The extent to which the transition is avoided in real liquids is thus controlled by the concentration of *localized* modes (involving a finite number of particles), which is found to be highly system-dependent.

We first present our central result and then provide its numerical support. Further details are given in the Supplemental Material (SM). In Fig. 1 we show results of force-minimizations that locate stationary and quasi-stationary points of the PES (the distinction between these two families [18] does not affect our conclusions, see SM). Diagonalization of the Hessian matrix yields a set of $3N$ eigenmodes, of which n_u corresponds to negative eigenvalues λ , i.e., to unstable directions. The top panel shows the corresponding average fraction of unstable modes $f_u = n_u/(3N)$ as a function of temperature T for several models of glass-forming liquids. They include binary [28] and ternary [29] soft spheres mixtures, as well as two models with continuous size polydispersity [27]. Most of these models have been equilibrated below their respective MCT crossover temperatures T_{MCT} , as determined from power-law fits of the relaxation time data [27, 30]. We are thus in a position to probe the landscape properties in a temperature range inaccessible to previous studies. At low temperature, we observe marked system-dependent deviations from an empirical power-law singularity introduced in Ref. [16]. Most importantly, the fraction of unstable modes is insensitive to the crossover and remains finite far below T_{MCT} , with barely any system-size dependence (see SM).

The picture changes qualitatively when the spatial lo-

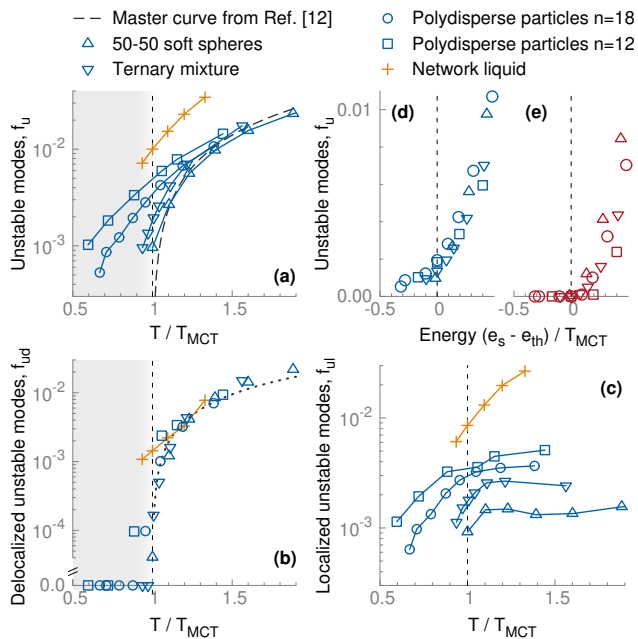


FIG. 1. Fractions of unstable modes in stationary and quasi-stationary points for all studied models. Rescaled temperature dependence of (a) total fraction f_u of unstable modes with dashed line from Ref. [16]. (b) Fraction f_{ud} of delocalized unstable modes. The dotted line is a linear function, Eq. (1), with $f_0 = 0.019$. (c) Fraction of localized modes. (d) f_u as a function of the scaled energy $(e_s - e_{th})/T_{MCT}$ of the stationary points. Temperature is used as an implicit variable. (e) Same as (d) for delocalized modes.

calization of the modes is taken into account. As described below, we distinguish between localized and delocalized unstable modes using a finite size scaling procedure. The fraction of delocalized unstable modes, f_{ud} , goes strictly to zero when the temperature drops below T_{MCT} , see Fig. 1(b). Because size effects are by construction taken into account, f_{ud} is representative of the thermodynamic limit and $f_{ud}(T < T_{MCT}) = 0$. The approach to T_{MCT} is approximately linear

$$f_{ud} = f_0 (T/T_{MCT} - 1), \quad \text{if } T > T_{MCT}. \quad (1)$$

We emphasize that the values of T_{MCT} were independently determined from power law fits to the dynamic data in previous work [27]. As in mean-field, a sharp geometric transition occurs indeed at T_{MCT} , but it captures the disappearance of delocalized unstable modes only. In finite dimensions, localized modes exist at any temperature and therefore the MCT crossover coincides with a localization transition of unstable modes.

The disappearance of delocalized modes implies that only localized modes survive below T_{MCT} . Figure 1(c) shows that the concentration of localized unstable modes $f_{ul} = (f_u - f_{ud})$ is highly system-dependent. We suggest that a higher fraction of localized modes at T_{MCT} corresponds to stronger deviations from the mean-field glassy scenario. Liquids that narrowly avoid the geomet-

ric transition may display a marked dynamic crossover from a regime governed by growing dynamic correlations, due to the delocalized unstable modes, to one where dynamic correlations build up instead from localized excitations and activated processes. Evidence of dynamic crossovers has been reported in experiments [31, 32] and more recently in simulations [33–36], but their microscopic physical origin remains to be assessed. Finally, the trend in Fig. 1(c) superficially suggests a correlation between glass-forming ability [27] and the concentration of localized unstable modes. While intriguing, this observation needs to be tested over a more diverse pool of liquids and also changing the dimensionality of space.

In mean-field p -spin models, the geometric transition is defined through the relationship between f_u and the energy e_s of stationary points. At the transition, stationary points of average energy e_{th} have a vanishing fraction of unstable modes f_u : $f_u(e_{th}) = 0$ [11]. Such a representation reveals an intrinsic property of the landscape and does not depend on the way in which the latter is sampled. In finite-dimensional systems, the $e_s(f_u)$ relation deviates from the linear behavior observed well above T_{MCT} [22, 23] and we confirm these results over a broader temperature range, see Fig. 1(d). These deviations were previously attributed to finite size effects [37], but they actually stem from localized modes. In fact, looking at the relation $e_s(f_{du})$ in Fig. 1(e), where the temperature is used as an implicit variable, one observes a sharp geometric transition at a finite energy threshold. This behavior is confirmed in all of the models (except the strong network-forming liquid, see below), and is a direct consequence of the localization transition. Below T_{MCT} , we observe small discrepancies between the localization properties of stationary points and quasi-stationary points, see SM for more details. This does not change the overall picture, since the localization properties of these two kinds of points are almost identical above T_{MCT} .

One notable deviation from the pattern described above occurs for a model of a strong tetrahedral network liquid [30], which mimics the structure and dynamics of silica. Even though the vast majority of unstable modes of this model is localized at any temperature [30], a small fraction of delocalized modes survive even below the putative MCT crossover and no geometric transition is found. This discrepancy is in line with the conventional Angell picture, which asserts that fragile and strong liquids form two distinct classes [1]. We argue that even if an underlying geometric transition were present in this model, its features would be washed out by the large concentration of localized modes, which corresponds to the elementary rearrangements of the tetrahedral structural units [30]. At a more fundamental level, our results cast doubts on the relevance of the MCT description of the early stages of glassy dynamics in strong liquids [38, 39], see also [40].

The results presented above rely on our ability to determine the mobility edge of the spectrum, *i.e.* the eigenvalue λ_e that separates localized and delocalized unstable

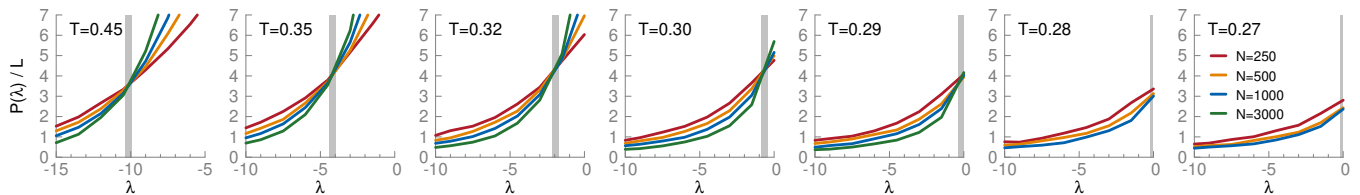


FIG. 2. Scaled participation ratio $P(\lambda, N)/L$ for all studied temperatures and system sizes N for the ternary mixture model. The mobility edge λ_e is the eigenvalue at which $P(\lambda, N)/L$ has a fixed point and is indicated by a vertical bar, showing that $\lambda_e(T \rightarrow T_{\text{MCT}}) = 0$.

modes. Early attempts to determine the mobility edge from the spectrum of the instantaneous normal modes (INM) in liquids were unsuccessful [41], but the technical problems were recently solved [42] by applying a finite-size scaling procedure borrowed from the study of Anderson localization [43]. We used this procedure to classify the unstable modes of all studied models. In the following, we illustrate this approach for one specific ternary mixture [29] and provide full details about the remaining systems in SM. We choose the ternary mixture model as a bench-case because it can be equilibrated below T_{MCT} with swap MC and we could gather good statistics on stationary points.

As a measure of the localization of a mode α , we consider the participation ratio

$$P_\alpha = \left(\sum_{i=1}^N |\vec{e}_{\alpha,i}|^4 \right)^{-1},$$

where $\vec{e}_{\alpha,i}$ is the corresponding normalized eigenvector. We then compute the average participation ratio $P(\lambda, N)$ of modes with eigenvalue λ for a given system size N . A finite-size scaling analysis allows one to determine the mobility edge λ_e as the fixed point in $P(\lambda, N)/L$, where L is the linear size of the system [42]. The rationale is that, for delocalized modes, P scales at least linearly with L whereas it is independent of L for localized modes. As a result, the mobility edge identifies the eigenvalue where finite size effects change nature. Localized modes have $\lambda < \lambda_e$, while $\lambda_e < \lambda < 0$ for delocalized modes.

Figure 2 shows the distribution of $P(\lambda, N)/L$ across the MCT crossover temperature. A well-defined fixed point at $\lambda_e(T)$ is visible in the participation ratio when $T > T_{\text{MCT}}$, and the data indicate that $\lambda_e(T \rightarrow 0.29) \rightarrow 0$, which matches precisely $T_{\text{MCT}} \approx 0.29$ determined from the dynamics [27]. Below this temperature, the absence of a non-trivial fixed point means that all unstable modes are localized. The fraction of delocalized and localized modes shown in Fig. 1 are then defined as $f_{ud} = \int_{\lambda_e}^0 g(\lambda) d\lambda$ and $f_{ul} = \int_{-\infty}^{\lambda_e} g(\lambda) d\lambda$, respectively, where $g(\lambda)$ is the normalized spectrum of the stationary points [44]. We used the largest system size available for each system to compute the fractions of unstable modes. Results obtained using INM showed instead that the vast majority of the unstable directions are delocalized at any temperature [42], with no obvious change

as $T \rightarrow T_{\text{MCT}}$. The INM thus seem unable to capture changes in the landscape properties relevant to the MCT crossover, unless perhaps by carefully filtering the unstable directions [45].

To corroborate our localization analysis, we consider two additional aspects: the shape of the unstable portion of the spectrum $g(\lambda)$ and its level spacing statistics. Following Ref. [46], we expect the unstable portion of the spectrum to behave differently depending on localization properties. For $\lambda_e < \lambda < 0$ and $T > T_{\text{MCT}}$, the spectrum should display a power-law behavior $g(\lambda) = A(\lambda - \lambda_0)^\nu$. This functional form is found in the mean-field p -spin model and, according to the single-saddle model of Ref. [46], is compatible with the short-time dynamics predicted by mode-coupling theory. Thus, it should describe well the delocalized portion of the spectrum $g(\lambda)$ in the MCT regime. For $\lambda < \lambda_e$, we expect instead an exponential tail $g(\lambda) = A \exp(-B\lambda)$, corresponding to an uncorrelated distribution of localized modes. In Fig. 3 we confirm the presence of these two regimes in the spectrum of the stationary and quasi-stationary points sampled at $T = 0.35 > T_{\text{MCT}}$. We notice that the crossover between them occurs very close to, though somewhat below, the mobility edge $\lambda_e(T = 0.35) \approx -4.1$ determined from the finite size scaling analysis. On the other hand, for $T < T_{\text{MCT}}$, the distribution is close to an exponential, as expected for a fully localized spectrum. Note that the shape of the unstable spectrum of stationary

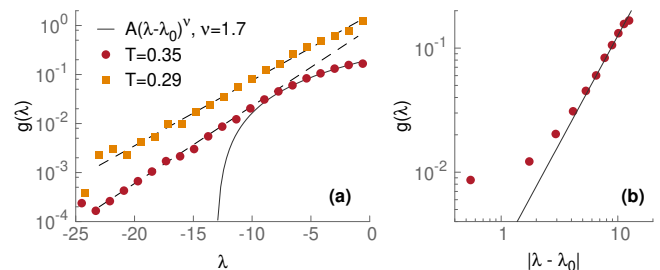


FIG. 3. Unstable part of the spectrum $g(\lambda)$ of stationary points for the ternary mixture. (a) $g(\lambda)$ at $T = 0.35$ and $T = 0.29$. For clarity the data for $T = 0.29$ are scaled by a factor 5. Dashed lines and full lines indicate fits to exponential and power law functions, respectively. (b) Power law behavior of $g(|\lambda - \lambda_0|)$ for $T = 0.35$, where λ_0 is obtained from the fit in (a).

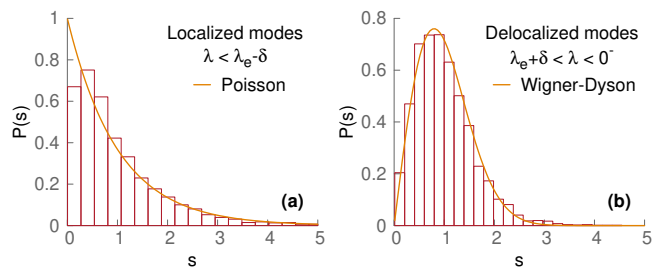


FIG. 4. Level spacing statistics at $T = 0.35$ for (a) localized and (b) delocalized modes in the ternary mixture model. The distribution $P(s)$ of level spacings s is computed in the indicated portion of eigenvalues, with $\delta = 1$. The full line indicates a Poisson distribution in (a) and a Wigner-Dyson distribution in (b).

points is quite distinct from the one, $g(\omega) \sim \omega^4$, found for soft stable modes [47]. It would be interesting to analyze more carefully the relationship between the unstable modes and the soft stable modes.

A well-established method to distinguish localized and delocalized modes builds on the analysis of the level spacing statistics [48], as used extensively in the analysis of spectra in a variety of problems, including the INM of supercooled and confined liquids [42, 49, 50]. Here we compute the level spacing distribution of stationary and quasi-stationary points of the PES. We first determine the smooth part of the cumulative density of states $\xi(\lambda)$ through a cubic spline of the raw data and then compute the level spacings $\tilde{s} = \xi(\lambda_{i+1}) - \xi(\lambda_i)$ from the ordered set of the eigenvalues. Finally, the level spacings are normalized, $s = \tilde{s}/\langle \tilde{s} \rangle$. In Fig. 4 we show representative results for the level spacing distribution at $T = 0.35$, i.e. in a regime where both kinds of modes can be clearly identified. We find that the level spacing distribution of the delocalized modes $\lambda > \lambda_e$ is well described by the Wigner-Dyson distribution

$$P(s) = \left(\frac{\pi s}{2}\right) \exp\left(-\frac{\pi}{4}s^2\right).$$

For the localized modes, the distribution is close to the Poisson distribution expected for uncorrelated eigenvalues, $P(s) = \exp(-s)$, although there remains a small depletion at small level spacings. The trend of the distributions for varying N (not shown) suggests that this depletion may be due to finite size effects. Overall, the analysis of the level spacing statistics confirms the localization transition of the unstable modes.

Finally, we make a direct contact with the real space structure of the modes and inspect the average displacements on the unstable modes $e_i^2 = (1/n_u) \sum_{\alpha} |\vec{e}_{\alpha,i}|^2$. Since each eigenvector is normalized, we have $e_i^2 < 1$. By averaging over all unstable modes, the instability field e_i^2 effectively captures the degree of localization of a given stationary point. The three snapshots in Fig. 5 depict the spatial distribution of e_i^2 for representative saddle points. On approaching T_{MCT} , the instability field e_i^2 becomes

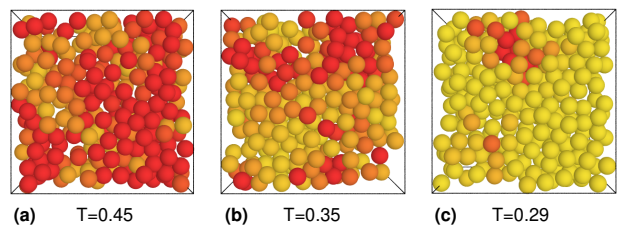


FIG. 5. Spatial distribution of the average displacements e_i^2 on the unstable modes for three stationary points sampled in the ternary mixture (a) well above ($T = 0.45$), (b) around ($T = 0.35$) and (c) at the mode-coupling temperature ($T = 0.29$). Only particles in a vertical slab of thickness 2σ are shown. The color coding interpolates between yellow (\bullet) for particles with $e_i^2 = 0$ and red (\bullet) for those with $e_i^2 \geq 0.04$.

more localized around few isolated particles with large displacements. Early simulations [51] found a correlation between this instability field and the short-time dynamical heterogeneity of a Lennard-Jones mixture. Our results suggest that the growth of dynamic correlations associated to the progressive stabilization of unstable modes as T approaches T_{MCT} is cut off because unstable modes become localized, which suggests a natural explanation for the non-monotonic evolution of dynamic correlations across T_{MCT} observed in some liquids [33–36].

In conclusion, the localization properties of unstable directions of the potential energy landscape of model glasses reveal a sharp localization transition in real space at the mode-coupling crossover temperature T_{MCT} . Our observations demonstrate that the geometric transition investigated in early work [9–11] applies rigorously only to the subset of delocalized unstable modes. This makes physical sense, since the mean-field models where the transition was first understood do not describe localized spatial fluctuations. In actual three-dimensional liquids, the geometric transition is in general avoided, because localized unstable modes exist at any temperature. The dynamic crossover predicted by mean-field theories across T_{MCT} will thus be clearly observed only in liquids that narrowly avoid the transition. In others, which includes in particular strong glass-formers, the physics should be dominated instead by localized excitations, associated to a higher concentration of localized unstable modes. Kinetically constrained models [52] could then provide an effective theoretical framework to account for the build up of dynamic correlations from such localized excitations. Liquids embedded in higher dimensions, which have recently received significant interest, are closer to mean-field behavior and we predict that they will display small concentrations of localized modes and be structurally very homogeneous. These expectations are consistent with recent numerical findings for a mean-field like three-dimensional model [53], and can now be tested numerically in large dimensions [54]. Future studies should also focus on generalizing the analysis to models of experimentally relevant models of molecular liquids.

ACKNOWLEDGMENTS

We thank W. Kob, M. Ozawa, G. Pastore and G. Tarjus for useful discussions. Data and workflow rele-

vant to this work will be available after publication at <https://doi.org/10.5281/zenodo.1478601>. This work was supported by a grant from the Simons Foundation (#454933, L. Berthier).

-
- [1] C. A. Angell, *Science* **267**, 1924 (1995).
 [2] L. Berthier and M. D. Ediger, *Phys. Today* **69**, 40 (2016).
 [3] A. Cavagna, *Phys. Rep.* **476**, 51 (2009).
 [4] L. Berthier and G. Biroli, *Rev. Mod. Phys.* **83**, 587 (2011).
 [5] C. P. Royall, F. Turci, S. Tatsumi, J. Russo, and J. Robinson, *J. Phys.: Condens. Matter* **30**, 363001 (2018).
 [6] W. Götze, *Complex Dynamics of Glass-Forming Liquids: A Mode-Coupling Theory* (Oxford University Press, USA, 2009).
 [7] T. R. Kirkpatrick and D. Thirumalai, *Phys. Rev. A* **37**, 4439 (1988).
 [8] A. Cavagna, *EPL (Europhysics Letters)* **53**, 490 (2001).
 [9] K. Broderix, K. K. Bhattacharya, A. Cavagna, A. Zippelius, and I. Giardina, *Phys. Rev. Lett.* **85**, 5360 (2000).
 [10] L. Angelani, R. Di Leonardo, G. Ruocco, A. Scala, and F. Sciortino, *Phys. Rev. Lett.* **85**, 5356 (2000).
 [11] T. S. Grigera, A. Cavagna, I. Giardina, and G. Parisi, *Phys. Rev. Lett.* **88**, 055502 (2002).
 [12] L. Angelani, R. Di Leonardo, G. Ruocco, A. Scala, and F. Sciortino, *J. Chem. Phys.* **116**, 10297 (2002).
 [13] G. Fabricius and D. A. Stariolo, *Phys. Rev. E* **66**, 031501 (2002).
 [14] J. Kurchan and L. Laloux, *J. Phys. A: Math. Gen.* **29**, 1929 (1996).
 [15] A. Cavagna, I. Giardina, and G. Parisi, *Phys. Rev. B* **57**, 11251 (1998).
 [16] L. Angelani, G. Ruocco, M. Sampoli, and F. Sciortino, *J. Chem. Phys.* **119**, 2120 (2003).
 [17] J. P. K. Doye and D. J. Wales, *J. Chem. Phys.* **116**, 3777 (2002).
 [18] J. P. K. Doye and D. J. Wales, *J. Chem. Phys.* **118**, 5263 (2003).
 [19] L. Berthier and J. P. Garrahan, *J. Chem. Phys.* **119**, 4367 (2003).
 [20] D. J. Wales and J. P. K. Doye, *J. Chem. Phys.* **119**, 12409 (2003).
 [21] B. Doliwa and A. Heuer, *Phys. Rev. E* **67**, 031506 (2003).
 [22] D. Coslovich and G. Pastore, *J. Chem. Phys.* **127**, 124505 (2007).
 [23] M. Ozawa, W. Kob, A. Ikeda, and K. Miyazaki, *PNAS* **112**, 6914 (2015).
 [24] D. Gazzillo and G. Pastore, *Chem. Phys. Lett.* **159**, 388 (1989).
 [25] T. S. Grigera and G. Parisi, *Phys. Rev. E* **63**, 045102 (2001).
 [26] L. Berthier, D. Coslovich, A. Ninarello, and M. Ozawa, *Phys. Rev. Lett.* **116**, 238002 (2016).
 [27] A. Ninarello, L. Berthier, and D. Coslovich, *Phys. Rev. X* **7**, 021039 (2017).
 [28] B. Bernu, J. P. Hansen, Y. Hiwatari, and G. Pastore, *Phys. Rev. A* **36**, 4891 (1987).
 [29] R. Gutiérrez, S. Karmakar, Y. G. Pollack, and I. Procaccia, *EPL* **111**, 56009 (2015).
 [30] D. Coslovich and G. Pastore, *J. Phys. Condens. Matter* **21**, 285107 (2009).
 [31] F. Stickel, E. W. Fischer, and R. Richert, *J. Chem. Phys.* **102**, 6251 (1995).
 [32] V. N. Novikov and A. P. Sokolov, *Phys. Rev. E* **92**, 062304 (2015).
 [33] W. Kob, S. Roldán-Vargas, and L. Berthier, *Nat. Phys.* **8**, 164 (2012).
 [34] L. Berthier, G. Biroli, D. Coslovich, W. Kob, and C. Toninelli, *Phys. Rev. E* **86**, 031502 (2012).
 [35] E. Flenner and G. Szamel, *J. Chem. Phys.* **138**, 12A523 (2013).
 [36] D. Coslovich, M. Ozawa, and W. Kob, *Eur. Phys. J. E* **41**, 62 (2018).
 [37] T. S. Grigera, *J. Chem. Phys.* **124**, 064502 (2006).
 [38] J. Horbach and W. Kob, *Phys. Rev. B* **60**, 3169 (1999).
 [39] F. Sciortino and W. Kob, *Phys. Rev. Lett.* **86**, 648 (2001).
 [40] L. Berthier, *Phys. Rev. E* **76**, 011507 (2007).
 [41] S. D. Bembenek and B. B. Laird, *J. Chem. Phys.* **104**, 5199 (1996).
 [42] V. I. Clapa, T. Kottos, and F. W. Starr, *J. Chem. Phys.* **136**, 144504 (2012).
 [43] B. I. Shklovskii, B. Shapiro, B. R. Sears, P. Lambrianides, and H. B. Shore, *Phys. Rev. B* **47**, 11487 (1993).
 [44] The three null modes as well the as spurious inflection mode of quasi-stationary points [17, 18] are removed from the analysis.
 [45] C. Donati, F. Sciortino, and P. Tartaglia, *Phys. Rev. Lett.* **85**, 1464 (2000).
 [46] A. Cavagna, I. Giardina, and T. S. Grigera, *J. Phys. A: Math. Gen.* **36**, 10721 (2003).
 [47] E. Lerner, G. Düring, and E. Bouchbinder, *Phys. Rev. Lett.* **117**, 035501 (2016).
 [48] T. Guhr, A. Müller-Groeling, and H. A. Weidenmüller, *Phys. Rep.* **299**, 189 (1998).
 [49] S. Ciliberti and T. S. Grigera, *Phys. Rev. E* **70**, 061502 (2004).
 [50] B. Ash, C. Dasgupta, and A. Ghosal, *Phys. Rev. E* **98**, 042134 (2018).
 [51] D. Coslovich and G. Pastore, *Europhys. Lett* **75**, 784 (2006).
 [52] A. Keys, L. O. Hedges, J. P. Garrahan, S. C. Glotzer, and D. Chandler, *Phys. Rev. X* **1**, 021013 (2011).
 [53] D. Coslovich, A. Ikeda, and K. Miyazaki, *Phys. Rev. E* **93**, 042602 (2016).
 [54] L. Berthier, P. Charbonneau, and J. Kundu, arXiv:1810.06950 (2018).

Supplemental Material for “The mode-coupling crossover of glasses is a localization transition”

Daniele Coslovich¹, Andrea Ninarello^{1,2}, Ludovic Berthier¹

¹*Laboratoire Charles Coulomb (L2C), University of Montpellier, CNRS, Montpellier, France*

²*CNR-ISC, Uos Sapienza, Piazzale A. Moro 2, 00185 Roma, Italy*

S1. MINIMIZATION PROTOCOL

We determined stationary and quasi-stationary points of the potential energy surface (PES) for systems of N point particles by minimizing the total squared force

$$W = \frac{1}{N} \sum_{i=1}^N |\vec{f}_i|^2 \quad (\text{S1})$$

where \vec{f}_i is the force on particle i . Minimizations start from instantaneous configurations obtained from Monte Carlo or molecular dynamics simulations at a given number density $\rho = N/V$ and temperature T . For each configuration, we used the l-BFGS minimization algorithm [1] to minimize W . It is well-known that W -minimizations locate *true* stationary points only rarely [2] and that the vast majority of points determined with this method are quasi-stationary points, at which there is precisely one inflection mode having a null zero eigenvalue [3]. In our minimizations, this inflection mode has a nearly zero eigenvalue whose norm $|\lambda|$ is typically between 10^{-6} and 10^{-4} (in the corresponding reduced units, see below) and which is clearly distinguishable from the lowest non-zero eigenvalue for the system sizes used in this work. The inflection mode was removed from the analysis, to avoid spurious $O(1/N)$ finite size effects when the fraction of unstable modes gets close to zero.

The stationary and quasi-stationary points can be distinguished from the corresponding value of W (in reduced units), which is low but non-zero for quasi-stationary points and zero within machine precision for true stationary points ($W \sim 10^{-14}$). In practice, we use a threshold of $\sim 10^{-10}$ to classify the two kinds of points for all models except for the polydisperse spheres with $n = 12$ (see below), for which a slightly higher threshold is used (3×10^{-9}) to account for a less strict convergence criterion on W -minimizations.

Previous studies showed that the statistical properties of quasi-stationary points and stationary points are practically indistinguishable above T_{MCT} [2]. We further discuss the similarity of these two kinds of points in Section S7.

Table S1 provides the reference values of the mode-coupling critical temperatures, obtained from power law fits to relaxation times data. We also report the threshold energies e_{th} , determined as the largest average energy of stationary points such that $f_{ud}(e_{th}) = 0$, where f_{ud} is the fraction of delocalized modes. Temperature is used as an implicit variable, $e_s = e_s(T)$.

Tables S2 to S6 provide details about the number of configurations analyzed for each temperature and number of particles, as well as the fraction of true stationary points (either saddles or minima) located by our minimizations.

TABLE S1. Mode-coupling temperatures T_{MCT} and threshold energies e_{th} . Note that for the network liquid the threshold energy could not be determined because $f_{ud} > 0$.

	50-50 soft spheres	Ternary mixture	Network liquid	Polydisperse $n = 18$	Polydisperse $n = 12$
T_{MCT}	0.20 [4]	0.288 [5]	0.31 [4]	0.50 [5]	0.104 [5]
e_{th}	1.74	1.077	–	1.468	0.243

S2. 50-50 SOFT SPHERES

This is the historical 50:50 binary mixture introduced by Bernu *et al.* [6]. The pair interaction potential is

$$u_{\alpha\beta}(r) = \epsilon \left(\frac{\sigma_{\alpha\beta}}{r} \right)^{12} \quad (\text{S2})$$

where $\alpha, \beta = A, B$ are species indexes. The size ratio is $\frac{\sigma_{AA}}{\sigma_{BB}} = 1.2$ and the cross-interaction term is additive $\sigma_{AB} = (\sigma_{AA} + \sigma_{BB})/2$. The potential is cutoff and shifted at a distance $r_{cut} = \sqrt{3}\sigma_{AA}$ by adding a cubic term that

ensures continuity of the potential up to the second derivative at r_{cut} [7, 11]. Energies and distances are expressed in units of ϵ and σ_{AA} , respectively. We used configurations from previous molecular dynamics simulations for N particles at a number density $\rho = N/V = 1$, with $N = 400, 800, 2000$ [4].

TABLE S2. Number of analyzed samples for the 50-50 soft sphere mixture. The number in parenthesis indicates the corresponding number of true stationary points obtained.

	$T = 0.2000$	$T = 0.2207$	$T = 0.2461$	$T = 0.2783$	$T = 0.3200$	$T = 0.3764$	$T = 0.4571$
$N = 500$	2800(24.1%)	3600(11.2%)	2000(12.0%)	800(15.8%)	800(17.5%)	2000(20.4%)	1000(19.5%)
$N = 1000$	3600(5.2%)	3600(2.3%)	800(3.1%)	800(7.0%)	800(9.4%)	800(9.4%)	400(7.2%)
$N = 2000$	1600(0.6%)	1600(0.0%)	800(0.6%)	800(3.0%)	800(4.8%)	800(4.2%)	400(5.0%)

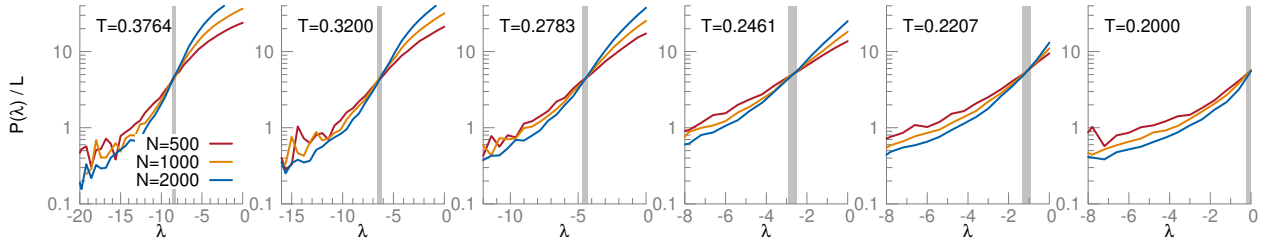


FIG. S1. Averaged scaled participation ratio as a function of eigenvalue λ for the 50-50 soft sphere mixture. Vertical arrows mark the mobility edge λ_e at a given temperature.

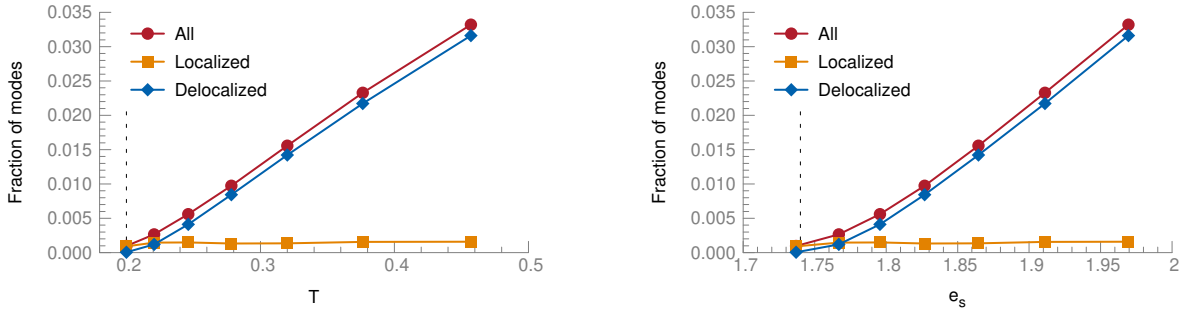


FIG. S2. Fraction of modes as a function of (a) temperature and (b) energy for the 50-50 soft sphere mixture ($N = 2000$). Vertical arrows in panel (a) and (b) mark the mode-coupling temperature T_{MCT} and the threshold energy e_{th} , respectively.

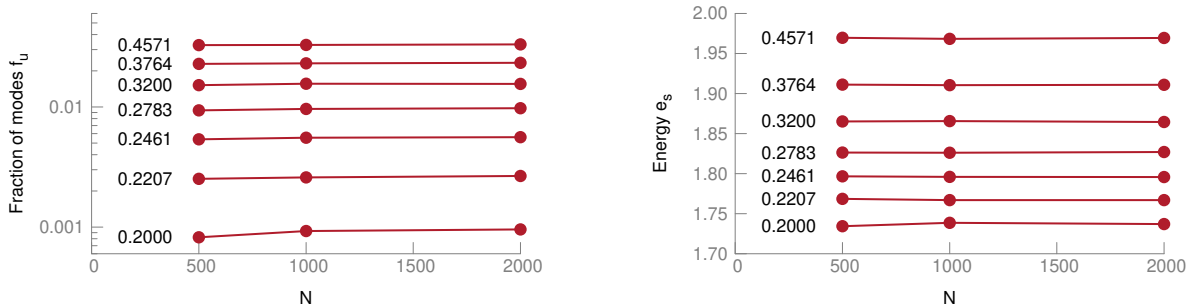


FIG. S3. (a) Fraction of modes and (b) energy of stationary points as a function of the number of particles N for the 50-50 soft sphere mixture

S3. TERNARY MIXTURE

The ternary mixture model studied in this work was introduced by Gutierrez *et al.* in Ref. [9]. The interaction potential is given by inverse power laws with an exponent 12, plus additional terms that ensure continuity of the derivatives at the cutoff:

$$u_{\alpha\beta}(r) = \left(\frac{\sigma_{\alpha\beta}}{r}\right)^{12} + c_4 \left(\frac{\sigma_{\alpha\beta}}{r}\right)^{-4} + c_2 \left(\frac{\sigma_{\alpha\beta}}{r}\right)^{-2} + c_0 \quad (\text{S3})$$

where $\alpha, \beta = A, B, C$. The expressions for c_0 , c_2 , and c_4 are given in [10]. The size ratio between two species is $\frac{\sigma_{AA}}{\sigma_{BB}} = \frac{\sigma_{BB}}{\sigma_{CC}} = 1.25$ and the chemical compositions are $x_A = 0.55$, $x_B = 0.30$, and $x_C = 0.15$. The potential is cut off at a distance $r_{cut} = 1.25\sigma_{\alpha\beta}$. We performed swap Monte Carlo simulations for $N = 250, 500, 1500, 3000$ particles at a number density $\rho = 1.1$. We used 80% of displacement moves over cubes of side $0.14\sigma_{AA}$ and 20% of swap moves [5]. To save computational time, we never attempted to exchange the identity of species A and C . We note that this model liquid can be equilibrated with swap Monte Carlo below the mode-coupling temperature $T_{MCT} = 0.29$ [5]. However, because of its crystallization tendency at low temperature, we could not simulate the metastable liquid with $N = 1500$ particles for $T < 0.27$ and the one with $N = 3000$ particles for $T < 0.28$. Energies and distances are expressed in units of ϵ and σ_{AA} , respectively.

TABLE S3. Number of analyzed samples for the ternary mixture. The number in parenthesis indicates the corresponding number of true stationary points obtained.

	$T = 0.27$	$T = 0.28$	$T = 0.29$	$T = 0.30$	$T = 0.32$	$T = 0.35$	$T = 0.45$
$N = 250$	5200(32.0%)	5200(22.6%)	5200(14.7%)	4000(10.8%)	4000(7.0%)	4000(6.6%)	4000(8.8%)
$N = 500$	4200(11.0%)	4086(6.1%)	4000(2.6%)	3400(1.5%)	3400(0.7%)	3400(1.2%)	3400(3.1%)
$N = 1000$	4400(1.2%)	4400(0.3%)	4400(0.1%)	4000(0.1%)	4000(0.0%)	4000(0.1%)	4000(0.8%)
$N = 3000$	0()	0()	450(0.0%)	450(0.0%)	450(0.0%)	180(0.0%)	90(0.0%)

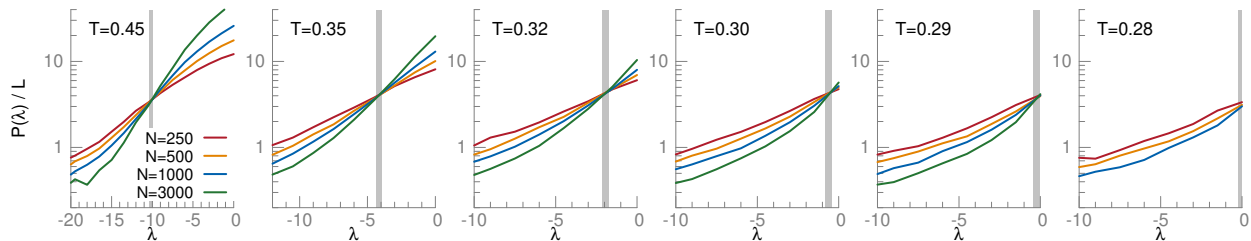


FIG. S4. Averaged scaled participation ratio as a function of eigenvalue λ for the ternary mixture. Vertical arrows mark the mobility edge λ_e at a given temperature.

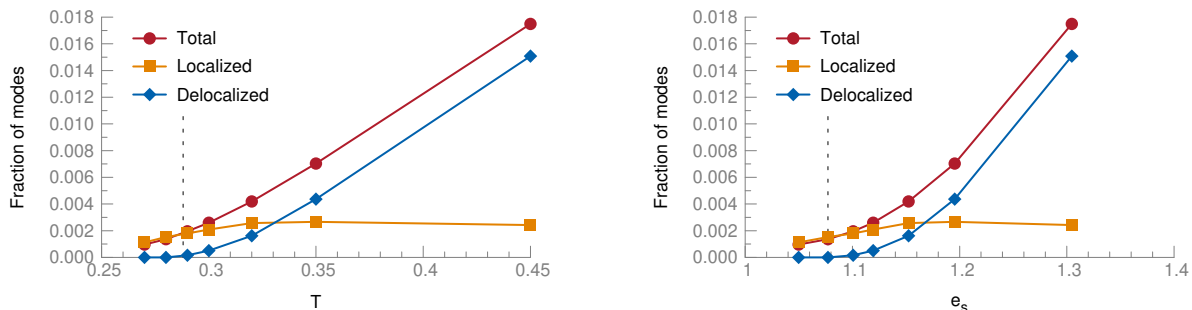


FIG. S5. Fraction of modes as a function of (a) temperature and (b) energy for the ternary mixture ($N = 1000$). Vertical arrows in panel (a) and (b) mark the mode-coupling temperature T_{MCT} and the threshold energy e_{th} , respectively.

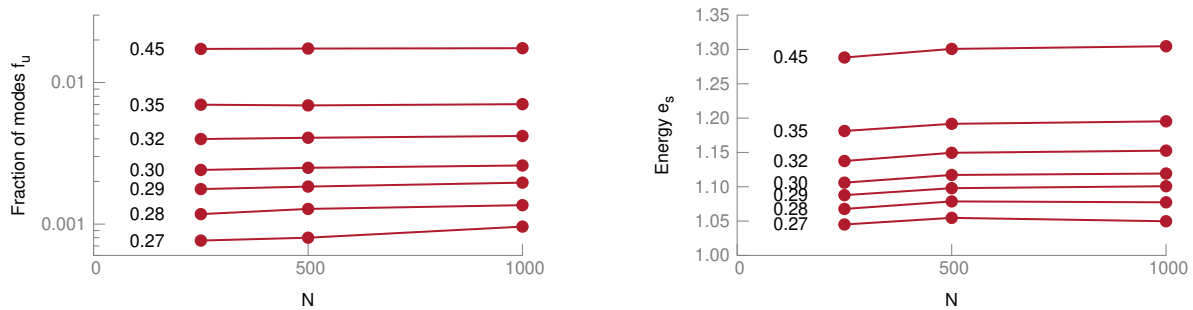


FIG. S6. (a) Fraction of modes and (b) energy of stationary points as a function of the number of particles N for the ternary mixture

S4. NETWORK LIQUID

The network liquid model is a simple binary mixture that mimics the structure and dynamics of silica [11]. The interaction potential between unlike species ($\alpha \neq \beta$) is of the Lennard-Jones type

$$u_{\alpha\beta}(r) = 4\epsilon_{\alpha\beta} \left[\left(\frac{\sigma_{\alpha\beta}}{r} \right)^{12} - \left(\frac{\sigma_{\alpha\beta}}{r} \right)^6 \right] \quad (\text{S4})$$

while the one between equal species is a simple inverse power

$$u_{\alpha\alpha} = \epsilon_{12}(\sigma/r)^{12} \quad (\text{S5})$$

Energies and distances are expressed in units of ϵ_{AA} and σ_{AA} , respectively. The remaining interaction parameters are $\epsilon_{AB} = 6$, $\sigma_{AB} = 0.49$, $\sigma_{BB} = 0.85$, $\epsilon_{BB} = 1$. The potential is cut off smoothly at r_{cut} by adding a cubic term that ensures continuity of the second derivative at the cut off distance r_{cut} , as for the soft sphere mixture [8]. The resulting cut-off distances are 2.07692, 1.39081, 1.76538 for $A-A$, $A-B$ and $B-B$ interactions, respectively. We analyzed simulations for system sizes $N = 400, 800, 2000$ at a number density $\rho = 1.655$ obtained from previous molecular dynamics simulations [4].

TABLE S4. Number of analyzed samples for the tetrahedral network liquid. The number in parenthesis indicates the corresponding number of true stationary points obtained.

	$T = 0.2900$	$T = 0.3100$	$T = 0.3397$	$T = 0.3716$	$T = 0.4120$
$N = 400$	1200(0.1%)	1200(0.0%)	1200(0.0%)	1200(0.0%)	400(0.0%)
$N = 800$	1200(0.0%)	1200(0.0%)	1200(0.0%)	1200(0.0%)	400(0.0%)
$N = 2000$	800(0.0%)	800(0.0%)	800(0.0%)	799(0.0%)	395(0.0%)

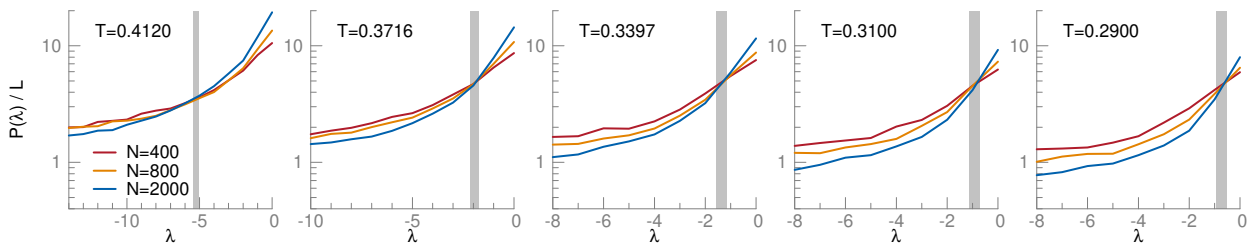


FIG. S7. Averaged scaled participation ratio as a function of eigenvalue λ for the tetrahedral network liquid. Vertical arrows mark the mobility edge λ_e at a given temperature.

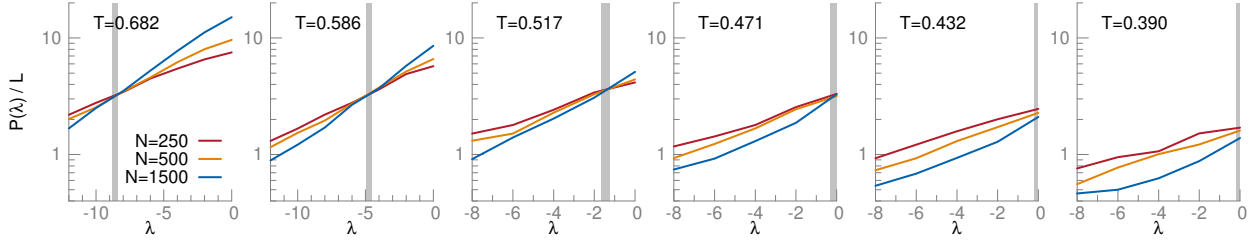


FIG. S10. Averaged scaled participation ratio as a function of eigenvalue λ for polydisperse soft spheres with $n = 18$. Vertical arrows mark the mobility edge λ_e at a given temperature.

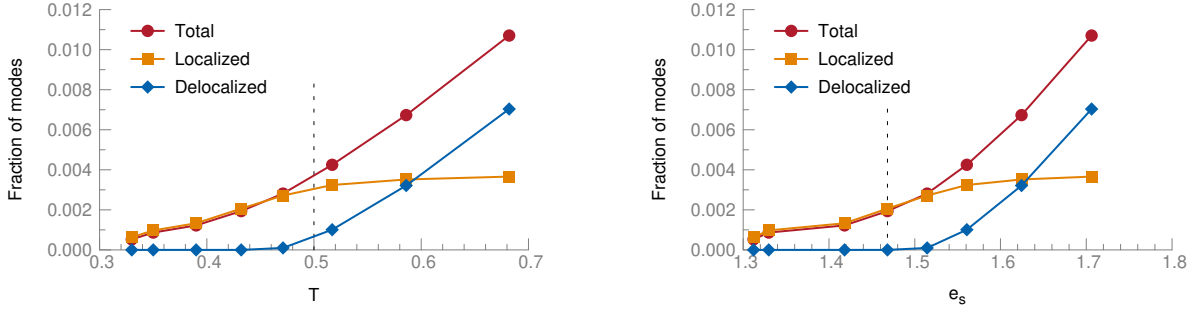


FIG. S11. Fraction of modes as a function of (a) temperature and (b) energy for the polydisperse soft spheres with $n = 18$ ($N = 1500$). Vertical arrows in panel (a) and (b) mark the mode-coupling temperature T_{MCT} and the threshold energy e_{th} , respectively.

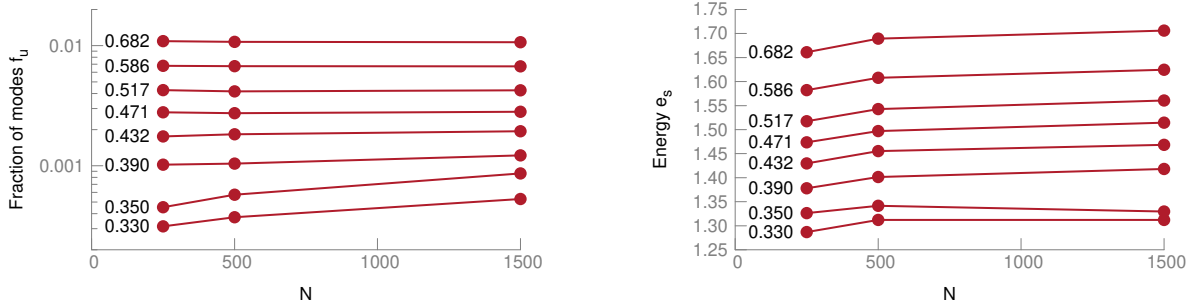


FIG. S12. (a) Fraction of modes and (b) energy of stationary points as a function of the number of particles N for the polydisperse soft spheres with $n = 18$

S6. POLYDISPERSE PARTICLES $N=12$

This is a variant of the polydisperse mixture introduced in the previous section. It features non-additive interactions to stabilize the fluid against phase separation [5]. The interaction potential between particles i and j is

$$u(r_{ij}) = \epsilon(\sigma_{ij}/r_{ij})^n + c_4 \left(\frac{r_{ij}}{\sigma_{ij}}\right)^4 + c_2 \left(\frac{r_{ij}}{\sigma_{ij}}\right)^2 + c_0 \quad (\text{S8})$$

with $n = 12$ and $\sigma_{ij} = (1 - 0.2|\sigma_i - \sigma_j|)(\sigma_i + \sigma_j)/2$. The coefficients c_0, c_2, c_4 are determined to ensure continuity of the potential at the cut-off distance $r_{cut} = 1.25\sigma_{ij}$. We use $\sigma_{max}/\sigma_{min} = 2.219$ which implies $\delta \approx 23\%$. We simulated systems composed of $N = 500, 1000, 1500$ particles at a number density $\rho = 1$ using the swap Monte Carlo algorithm described in Ref. [5].

TABLE S6. Number of analyzed samples for the polydisperse soft spheres with $n = 12$. The number in parenthesis indicates the corresponding number of true stationary points obtained.

	$T = 0.062$	$T = 0.075$	$T = 0.092$	$T = 0.110$	$T = 0.120$	$T = 0.150$
$N = 250$	1000(19.1%)	1000(5.5%)	1000(0.5%)	1000(0.2%)	1000(0.1%)	1000(0.2%)
$N = 500$	1000(5.0%)	1000(0.5%)	1000(0.0%)	1000(0.0%)	1000(0.0%)	1000(0.0%)
$N = 1500$	400(0.0%)	400(0.0%)	400(0.0%)	400(0.0%)	400(0.0%)	400(0.0%)

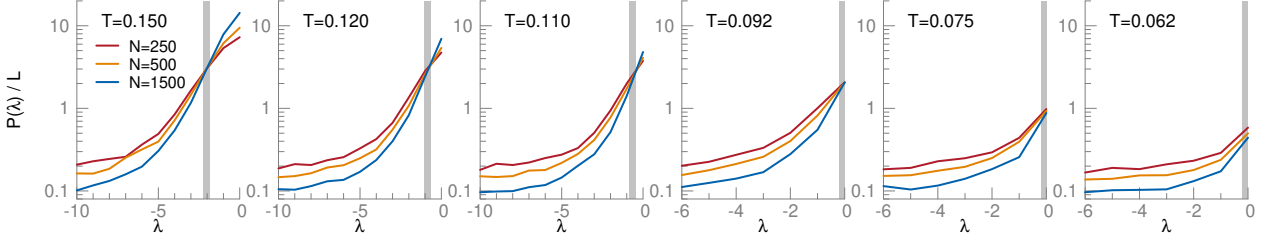


FIG. S13. Averaged scaled participation ratio as a function of eigenvalue λ for the polydisperse soft spheres with $n = 12$. Vertical arrows mark the mobility edge λ_e at a given temperature.

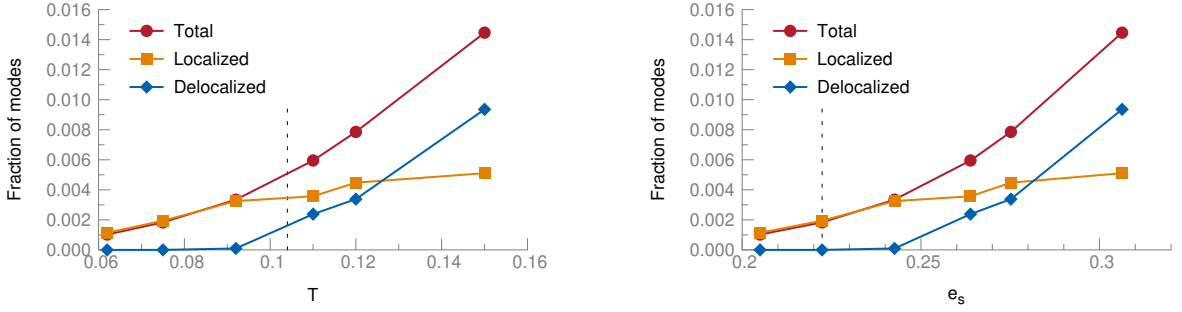


FIG. S14. Fraction of modes as a function of (a) temperature and (b) energy for the polydisperse soft spheres with $n = 12$ ($N=1500$). Vertical arrows in panel (a) and (b) mark the mode-coupling temperature T_{MCT} and the threshold energy e_{th} , respectively.

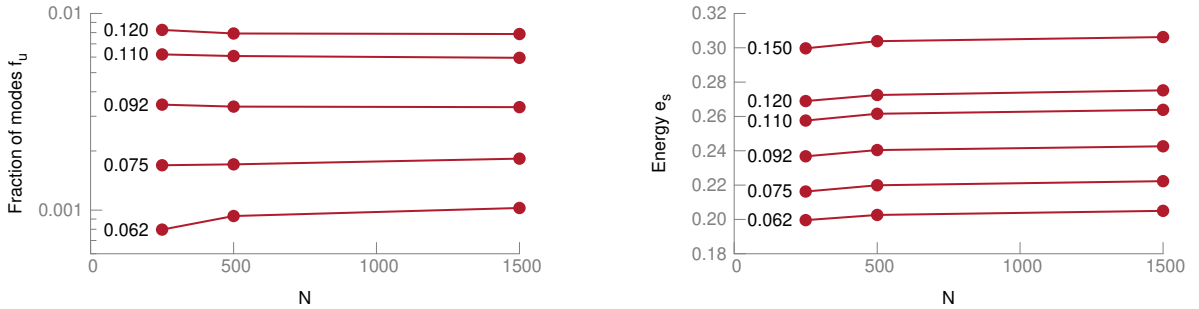


FIG. S15. (a) Fraction of modes and (b) energy of stationary points as a function of the number of particles N for the polydisperse soft spheres with $n = 12$

S7. QUASI-STATIONARY POINTS VERSUS STATIONARY POINTS

In this section we compare the statistical properties of quasi-stationary and stationary points for the ternary mixture. We focus on this model because it is the one for which we accumulated the largest statistics.

The geometric plot $e_s(f_u)$ in Fig. S16 shows results obtained separately for stationary points and for the bulk of the points obtained from W -minimizations. Only minor discrepancies between the two sets of data are visible, the fraction of unstable modes being slightly smaller in stationary points at small e_s .

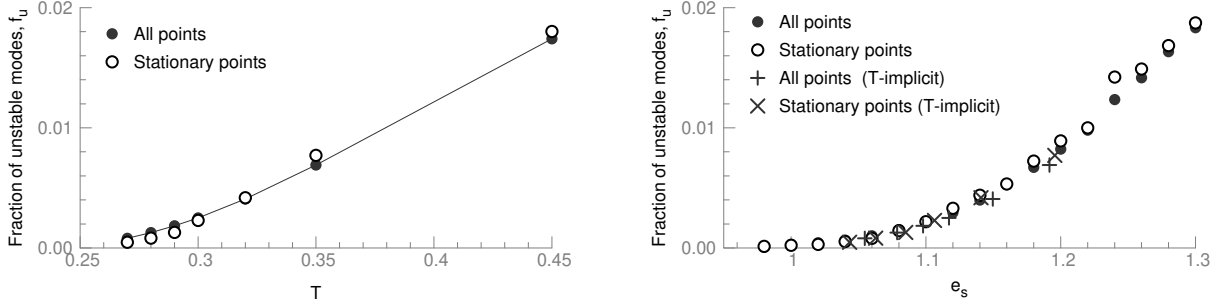


FIG. S16. Fraction of unstable modes in all points and in true stationary points obtained from W -minimizations as function of (a) temperature and (b) energy. In panel (b) we show both averages on a per-energy basis and using T as an implicit variable. The number of particles is $N = 500$.

In Fig. S17 we show the participation ratio $P(\lambda)$ of the unstable modes for all points obtained from all W -minimizations and for stationary points only. The two sets of data are consistent with one another above the mode-coupling temperature $T_{\text{MCT}} = 0.29$ but they differ slightly around and below this temperature. Unstable modes of stationary points are slightly more localized than the ones of quasi-stationary points at low temperature. A plot of the average participation ratio as a function of the fraction f_u shows a good data collapse of the two sets of data (not shown).

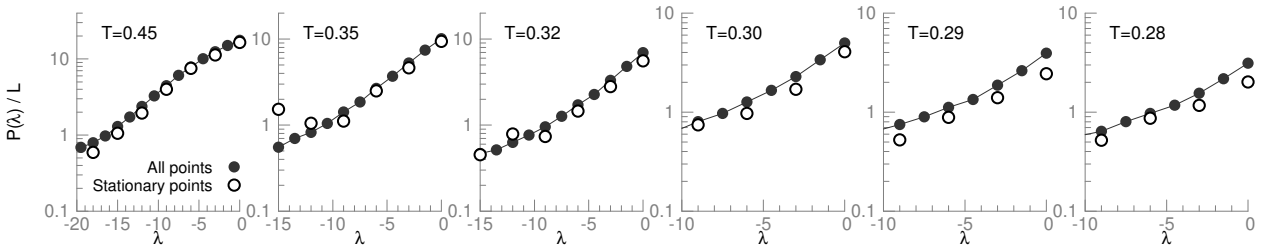


FIG. S17. Scaled participation ratio $P(\lambda)/L$ as a function of λ for the ternary mixture for all points obtained from W -minimizations (filled circles) and for stationary points only (empty circles). The number of particles is $N = 500$.

In Fig. S18 we show the fraction of delocalized unstable modes for stationary points only, *i.e.* without quasi-stationary points. We use the mobility edge obtained from analysis of all W -minimizations because the current statistics on the participation ratio is not sufficient to determine the mobility edge. We observe small deviations close to the mode-coupling temperature with respect to the approximate master curve $f_{ud}(T) = 0.019(T/T_{\text{MCT}} - 1)$ determined from all the points. Overall the trend confirms a sharp localization transition of the stationary points at the mode-coupling temperature.

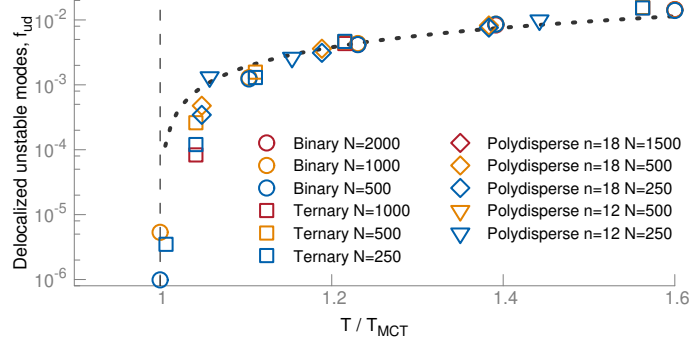


FIG. S18. Fraction of delocalized unstable modes f_{ud} as a function of T/T_{MCT} for stationary points only, in all studied models except the network-forming liquid. The system size N is indicated in the legend. The dotted line indicates the approximate master curve, Eq.1 in the main text, obtained from all points.

-
- [1] D. C. Liu and J. Nocedal, *Math. Program.* **45**, 503 (1989).
 - [2] L. Angelani, R. Di Leonardo, G. Ruocco, A. Scala, and F. Sciortino, *J. Chem. Phys.* **116**, 10297 (2002).
 - [3] J. P. K. Doye and D. J. Wales, *J. Chem. Phys.* **116**, 3777 (2002).
 - [4] L. Berthier, G. Biroli, D. Coslovich, W. Kob, and C. Toninelli, *Phys. Rev. E* **86** (2012).
 - [5] A. Ninarello, L. Berthier, and D. Coslovich, *Phys. Rev. X* **7**, 021039 (2017).
 - [6] B. Bernu, J. P. Hansen, Y. Hiwatari, and G. Pastore, *Phys. Rev. A* **36**, 4891 (1987).
 - [7] T. S. Grigera and G. Parisi, *Phys. Rev. E* **63**, 045102 (2001).
 - [8] T. S. Grigera, A. Cavagna, I. Giardina, and G. Parisi, *Phys. Rev. Lett.* **88**, 055502 (2002).
 - [9] R. Gutiérrez, S. Karmakar, Y. G. Pollack, and I. Procaccia, *EPL* **111**, 56009 (2015).
 - [10] S. Karmakar, E. Lerner, I. Procaccia, and J. Zylberg, *Phys. Rev. E* **83**, 046106 (2011).
 - [11] D. Coslovich and G. Pastore, *J. Phys. Condens. Matter* **21**, 285107 (2009).